Biomaterials 31 (2010) 9422–9430

Contents lists available at ScienceDirect

Biomaterials

journal homepage: www.elsevier.com/locate/biomaterials

Phosphorylation-dependent mineral-type specificity for apatite-binding peptide sequences

William N. Addison [a], Sharon J. Miller [b], Janani Ramaswamy [b], Ahmad Mansouri [a], David H. Kohn [b,c,*], Marc D. McKee [a,d,**]

[a] Faculty of Dentistry, McGill University, Montreal, QC, Canada
[b] Dept. of Biomedical Engineering, University of Michigan, Ann Arbor, MI, USA
[c] Dept. of Biologic and Materials Sciences, University of Michigan, Ann Arbor, MI, USA
[d] Dept. of Anatomy and Cell Biology, McGill University, Montreal, QC, Canada

ARTICLE INFO

Article history:
Received 30 July 2010
Accepted 25 August 2010
Available online 12 October 2010

Keywords:
Phage display
Bone mineral
Peptides
Apatite
Osteoblast
Phosphorylation

ABSTRACT

Apatite-binding peptides discovered by phage display provide an alternative design method for creating functional biomaterials for bone and tooth tissue repair. A limitation of this approach is the absence of display peptide phosphorylation – a post-translational modification important to mineral-binding proteins. To refine the material specificity of a recently identified apatite-binding peptide, and to determine critical design parameters (net charge, charge distribution, amino acid sequence and composition) controlling peptide affinity for mineral, we investigated the effects of phosphorylation and sequence scrambling on peptide adsorption to four different apatites (bone-like mineral, and three types of apatite containing initially 0, 5.6 and 10.5% carbonate). Phosphorylation of the VTKHLNQISQSY peptide (VTK peptide) led to a 10-fold increase in peptide adsorption (compared to nonphosphorylated peptide) to bone-like mineral, and a 2-fold increase in adsorption to the carbonated apatite, but there was no effect of phosphorylation on peptide affinity to pure hydroxyapatite (without carbonate). Sequence scrambling of the nonphosphorylated VTK peptide enhanced its specificity for the bone-like mineral, but scrambled phosphorylated VTK peptide (pVTK) did not significantly alter mineral-binding suggesting that despite the importance of sequence order and/or charge distribution to mineral-binding, the enhanced binding after phosphorylation exceeds any further enhancement by altered sequence order. Osteoblast culture mineralization was dose-dependently inhibited by pVTK and to a significantly lesser extent by scrambled pVTK, while the nonphosphorylated and scrambled forms had no effect, indicating that inhibition of osteoblast mineralization is dependent on both peptide sequence and charge. Computational modeling of peptide–mineral interactions indicated a favorable change in binding energy upon phosphorylation that was unaffected by scrambling. In conclusion, phosphorylation of serine residues increases peptide specificity for bone-like mineral, whose adsorption is determined primarily by sequence composition and net charge as opposed to sequence order. However, sequence order in addition to net charge modulates the mineralization of osteoblast cultures. The ability of such peptides to inhibit mineralization has potential utility in the management of pathologic calcification.

1. Introduction

Biomimetic materials used in the repair of traumatic or pathologic bone and tooth defects endeavour to guide the regeneration of mineralized tissues by providing molecular cues to the damaged tissue. The inherent complexity of skeletal and dental tissues requires not only that biomaterials must elicit specific cellular responses that lead to extracellular matrix formation, but that the tissue formed must be both spatially and temporally controlled, and mineralizable. *In vivo*, highly coordinated temporo–spatial control is usually provided by biologic molecules and cell-to-cell

* Corresponding author. 2213 School of Dentistry, 1011 North University Avenue, Ann Arbor, MI, USA 48109-1078. Tel.: +1 734 764 2206; fax: +1 734 647 2110.
** Corresponding author. Faculty of Dentistry, McGill University, 3640 University Street Montreal, QC, Canada H3A 2B2. Tel.: +1 514 398 7203x00041; fax: +1 514 398 8900.
E-mail addresses: william.addison@mail.mcgill.ca (W.N. Addison), sharonjm@umich.edu (S.J. Miller), jananir@umich.edu (J. Ramaswamy), ahmad.mansouri@mail.mcgill.ca (A. Mansouri), dhkohn@umich.edu (D.H. Kohn), marc.mckee@mcgill.ca (M.D. McKee).

0142-9612/$ – see front matter © 2010 Elsevier Ltd. All rights reserved.
doi:10.1016/j.biomaterials.2010.08.064

communication, and therefore the incorporation of surface or soluble signals in the design of biomaterials is a logical approach to influence tissue development [1,2]. A central tenet of biomimetic material design for connective tissues is that replicating key aspects of natural extracellular matrices will enable materials to achieve a greater level of control over cell function, and allow better integration into host tissues.

The choice and design of biologic molecules potentially useful in any given physiologic milieu depends on factors that include the chemistry of the implantable material itself, and the type of defect in a target tissue. Current scaffolding/implant materials commonly used in orthopedic and dental applications – such as metals, calcium-phosphate ceramics and polymers – each present different surface chemistries, topographies and stiffness, and each have their inherent limitations and applications. Although mineral particles can be used directly to fill bone and tooth defects and enhance the osseointegration of implants [3], induction of bone formation generally requires additional modification by biologic molecules [4]. However, processing and design steps used to fabricate implantable materials often can be detrimental to incorporation of organic, biologic molecules into implants – an example being the commonly used high sintering temperatures used in the processing of implantable ceramics and composites. The biomimetic precipitation of bone-like mineral (BLM) is an alternative process that occurs at physiologic temperatures (37 °C) and is not destructive to any incorporated biologic components [5]. Biomimetically produced BLM in turn can provide a scaffold for the adsorption/incorporation or co-precipitation of biologic molecules such that biomolecular functions are retained and induction of osteogenesis can occur [6–8].

Modification of implantable surfaces with bioactive peptides is one approach to designing biomimetic materials. However, unlike polymeric and other materials, the surface of hydroxyapatite mineral is not easily modified by surface treatments that form functional hydroxyl-, amino, or carboxyl- groups commonly used in implant design; thus, there is a need for peptide sequences that preferentially adhere to this material/mineral surface. Furthermore, compared to full-length proteins, relatively smaller bioactive peptides are cheaper and faster to produce, easier to purify, and do not require processing from animal sources. Traditional design methods use peptide sequences adapted from mineral-binding proteins such as osteopontin, bone sialoprotein and statherin [9–11]. Mineral-binding sequences in these proteins are rich in acidic residues (aspartate, glutamate and phosphoserines) resulting in a net negative charge that promotes binding to positively charged calcium at apatite crystal faces [12,13]. These proteins, and peptides derived from them, often lack mineral-type specificity – a notable example being osteopontin which binds to and influences the growth of hydroxyapatite [14], calcium oxalate [15] and calcite [16]. Design of mineral-type specificity is considered advantageous for tissue-specific implantable materials, as these may result in better tissue integration and function. New design methods may also be applicable to the development of material-specific peptides to be used as molecular probes/sensors to identify mineral phases in pathologic crystal deposits, or even as targeting tags for delivery of drugs [17] or tissue-specific molecules.

Previously, we have used phage display to identify a 12-mer peptide sequence – VTKHLNQISQSY (hereafter called VTK) from a combinatorial library of 10^9 phages – that preferentially adsorbs to bone-like mineral and hydroxyapatite [18]. Phage display technology involves expressing a library of peptide sequences on the protein coat of a bacteriophage, and then panning for sequences that adhere to a ligand or substrate of interest [19]. Phage display has been used to identify peptide sequences that bind to proteins, DNA, cells, polymers, and even inorganic materials such as silver and titanium [19–22]. One limitation of phage display is the inability to include post-translational modifications within the peptides being expressed on the phage protein coat. Post-translational phosphorylation of serine, threonine and tyrosine residues are particularly important in proteins and peptides involved in the regulation of biomineralization [23]. Phosphorylation of serine residues is common in proteins involved in biomineralization, and VTK contains two serine residues with the potential for phosphorylation. Phosphorylation could provide a means to further improve peptide adsorption, modulate material specificity and modify cellular responses to the peptides.

In this study, we determined critical design parameters controlling peptide affinity to synthetic and biologic apatites by investigating the effects of phosphorylation and amino acid sequence scrambling on peptide–mineral-binding, and using a functional assay, examined their ability to inhibit osteoblast cell culture mineralization. We have also explored the mechanism underlying mineral-binding of these peptides by RosettaSurface computational simulations for peptide structure prediction at the surface of mineral. Collectively, these studies provide insight on the role of peptide charge, charge distribution, composition and amino acid sequence in the design of functional biomaterials.

2. Materials and methods

2.1. Preparation of biomimetic bone-like mineral films and apatite disks

To make a layer of bone-like mineral (BLM), a film of 5% (w/v) 85:15 polylactic-co-glycolic acid (PLGA, Alkermes)-chloroform solution was cast onto 12-mm diameter glass slide. Following overnight drying, the PLGA films were etched in 0.5 M NaOH for 7 min, rinsed in ddH_2O, and soaked in modified simulated body fluid (141 mM NaCl, 4.0 mM KCl, 0.5 mM $MgSO_4$, 1.0 mM $MgCl_2$, 4.2 mM $NaHCO_3$, 5.0 mM $CaCl_2.2H_20$, and 2.0 mM KH_2PO_4) at pH 6.8 for 5 days at 37 °C [8] to deposit a carbonated apatite layer on the PLGA substrate film. The modified simulated body fluid was changed daily to maintain supersaturation and thermodynamic conditions conducive to heterogeneous nucleation of mineral. Hydroxyapatite (HA) disks (10 mm in diameter × 4 mm thick) were pressed from powder (Plasma Biotal Ltd.) at 1 metric ton for 1 min and sintered at 1350 °C for 1 h.

Carbonated apatite disks were made from 5.6% (CA5) and 10.5% (CA10) carbonated apatite powders (a generous gift from Dr. Mary Tecklenburg [Central Michigan University]). Carbonated apatite disks (8–10 mm in diameter × 2–4 mm thick) were pressed from powders at 0.5 metric ton for 1 min and sintered at 1350 °C for 1 h (heating rate of 10 °C/min). HA and carbonated disks were sonicated in 10 mM HCl, then in ddH_2O. All sintered disks (CA5, CA10, and HA) were autoclaved prior to use. Macroscopic dimensions of all disks were measured with calipers. Carbonate content in CA5 and CA10 was reduced to ~2% after sintering. The morphology, composition, crystallinity and surface area of the materials have been characterized using scanning electron microscopy, Fourier-Transform Infrared Spectroscopy, X-ray diffraction, and Brunauer-Emmett Teller (BET) methods, respectively, and were previously reported [18].

2.2. Peptide synthesis

A peptide sequence – VTKHLNQISQSY (VTK) – with high and preferential affinity to apatite-based materials was previously discovered from phage display [18,24]. To investigate the role of residue charge, charge distribution and sequence as design parameters in controlling peptide affinity to synthetic and biologic apatite, phosphorylated (VTKHLNQIpSQpSY) and scrambled (IYQSKHTLSNQV; IYQpSKHTLpSNQV) variants of the VTK peptide were also studied. Scrambled sequences were obtained using a random number generator. All peptides were fabricated on a Rainin Symphony Synthesizer by Fmoc solid-phase chemistry according to standard peptide synthesis procedures and characterized as having >86% purity by high-performance liquid chromatography (University of Michigan Protein Core). Phosphorylations at specific serine residues in the peptide sequence were achieved using preformed, protected phosphoserine amino acids. For experiments involving fluorescence, peptides were labelled on resin before cleavage using 5-(and-6)-carboxyfluorescein succinimidyl ester (Molecular Probes C-1311) (University of Michigan Protein Core). The peptides used in this study, and some of their properties, are summarized in Table 1. Isoelectric points were calculated using Scansite [25] and the Compute pI/Mw tool on the ExPASy proteomics server [26].

2.3. Synthetic peptide adsorption assay

For each peptide, a UV absorbance value vs. absorbance wavelength graph was generated from 200 to 300 nm (BioRad Smartspec 3000). UV absorbance maxima for

Table 1
Amino acid sequences and isoelectric point (pI) of the peptides used in this study.

Peptide	Sequence	Description	Phosphates	Net Charge	pI
VTK	VTKHLNQISQSY	Apatite-specific peptide identified by phage display	0	+1	8.6
pVTK	VTKHLNQI(**pS**)Q(**pS**)Y	Phosphorylated VTK	2	−3	4.8
VTK-scram	IYQSKHTLSNQV	Scrambled VTK	0	+1	8.6
pVTK-scram	IYQ(**pS**)KHTL(**pS**)NQV	Scrambled phosphorylated VTK	2	−3	4.8

VTK were at 225 nm. From these graphs, the wavelength resulting in the highest UV absorbance for each peptide was used to generate standard curves (peptide concentration vs. UV absorbance) and estimations of peptide concentrations. Standard curves consisting of the concentrations 0, 1, 5, 10, 25, 50, 75, 100, 250, 500, 750, and 1000 μg/mL were developed for each peptide tested. From duplicate readings per concentration, the error introduced from the detection technique was ~5%. A modified standard curve consisting of values below 100 μg/mL was used for each peptide to calculate the unknown peptide amount that adsorbed onto each material tested. Amino acid analysis was performed to verify peptide concentration for standard curves created with UV absorbance at 205 nm and 225 nm wavelengths. Peptides were reconstituted in ddH_2O and diluted to ~500 μg/mL in 50 mM Trizma buffer, pH 7.5. BLM films, hydroxyapatite, CA5 and CA10 disks, and blank TCPS wells were soaked in ddH_2O overnight at 4 °C ($n = 5–6$ per material) in 24-well polystyrene tissue culture dishes. Prior to introducing 1 mL of the peptide or buffer solutions for negative controls, plates were allowed to warm to room temperature and then the overnight solution was removed. Plates were agitated on a Titer Plate Shaker at ~80 rpm for 3 h at room temperature. The films and disks were rinsed with ddH_2O and then soaked in a 10 mM HCl solution for 18 h at room temperature on the same shaker. To determine the amount of peptide adsorbed, aliquots of the HCl solution were read on a UV spectrophotometer.

2.4. Cell culture

MC3T3-E1 (subclone 14) murine calvarial osteoblasts [27] (courtesy of Dr. R. Franceschi, University of Michigan, Ann Arbor, MI, USA) were maintained in modified α-minimum essential media (Invitrogen) supplemented with 10% FBS (Hyclone) and 1% penicillin–streptomycin (Invitrogen) at 37 °C in a humidified atmosphere of 5% CO_2. All experiments were carried out at a plating density of 50,000 cells/cm^2. Cell differentiation and matrix mineralization were initiated 24 h after plating by replacing the medium with fresh medium supplemented with 50 μg/mL ascorbic acid (Sigma) and 10 mM β-glycerophosphate (Sigma). Medium, with or without peptide (see above), was changed every 48 h over a 12-day time period.

2.5. Quantification of mineralization

After 12 days of culture, mineral was visualized by von Kossa staining using 5% silver nitrate solution (Sigma). For quantification of mineralization by measuring calcium deposited within the cell/matrix layer, cultures were decalcified with 0.5 N HCl, and calcium in the supernatant was determined spectrophotometrically (absorbance at 595 nm) from duplicate readings per well using a calcium assay kit (Diagnostic Chemicals).

2.6. Assay for cell proliferation

Cell proliferation and viability in the presence of peptide were measured using the MTT assay [28]. Briefly, cells were incubated with 0.5 μg/μL MTT (3-[4,5-dimethylthiazol-2-yl]-2,5-diphenyl tetrazolium bromide) (Sigma) in medium for 3 h, solubilized with DMSO and absorbance measured at 562 nm.

2.7. Binding of fluorescently-labelled peptides to osteoblast culture mineral

Maximally mineralized day 12 osteoblast cultures were incubated with 150 μM of fluorescently-labelled peptide in culture medium for 1 h at room temperature. After washing three times with phosphate-buffered saline, cultures were incubated with 30 μM calcein blue (Sigma) for 1 h, dried and visualized a Leica DM IL inverted fluorescent microscope (Leica).

2.8. Computational modeling and energy calculations

All simulations were performed using the RosettaSurface Monte Carlo plus minimization structure prediction program [29]. Each execution of the program folds a peptide from a fully extended conformation and results in an energy-minimized solution- and adsorbed-state structure. Large structural ensembles of 10^5 candidate solution- and adsorbed-state conformers were generated from which only the 100 lowest-energy structures, from each state, were chosen for further analysis. Fully extended peptide structures were constructed with PyMOL (DeLano Scientific). Hydroxyapatite crystal surface with $P2_1/b$ space group, lattice parameters of $a = 9.42$, $b = 2a$, $c = 6.88$ and $\gamma = 120°$, and positive Ca^{2+} termination on the {100} crystallographic face was constructed with CrystalMaker (CrystalMaker Software Ltd.). The {100} face is a highly stable hydroxyapatite surface to which several mineralization-related proteins are known to bind [30,31].

2.9. Statistics

Data is presented as mean values ± one standard deviation. ANOVA on RANKS with Dunn's post-hoc comparisons (SigmaStat) were used to determine effect of peptide sequence on adsorption to each substrate. Effects of phosphorylation (differences between VTK and pVTK; VTK-scram and pVTK-scram) and scrambling (differences between VTK and VTK-scram; pVTK and pVTK-scram) were also determined from the Dunn's test. Independent sample *t*-tests were used to determine differences between VTK and pVTK on each material and differences in peptide adsorption between BLM and hydroxyapatite. *In vitro* quantification of mineralization and proliferation was assessed with Student's *t*-tests for effects of phosphorylation and scrambling (GraphPad Software). Experiments were performed in triplicate.

3. Results

3.1. Effect of phosphorylation on peptide adsorption to synthetic apatite-based substrates

Adsorption of VTKHLNQISQSY (VTK) and VTK phosphorylated at Ser-9 and Ser-11 (pVTK) to four apatite-based minerals and to tissue culture polystyrene (TCPS) was measured using a synthetic peptide adsorption assay. VTK and pVTK did not adsorb to TCPS (Fig. 1),

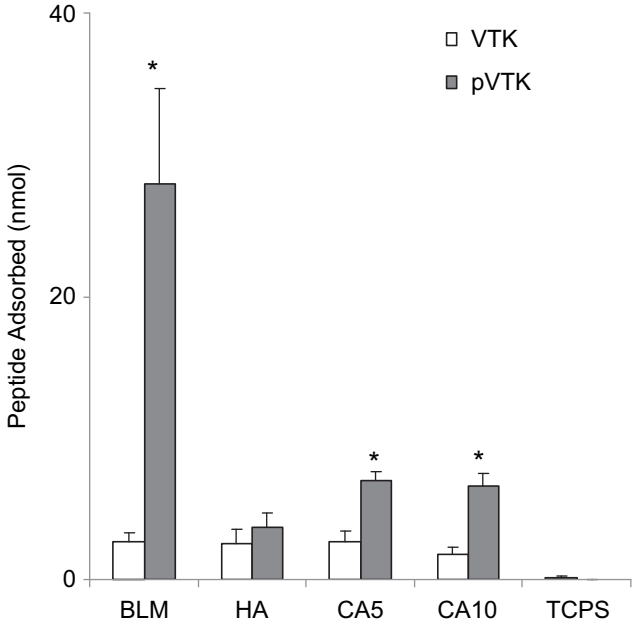

Fig. 1. Adsorption of VTK and phosphorylated VTK (pVTK) peptides on bone-like mineral (BLM) layer, and pressed and sintered disks prepared from hydroxyapatite (HA), 5.6% carbonated apatite (CA5), and 10.5% carbonated apatite (CA10), and tissue culture polystyrene (TCPS). Phosphorylating serine residues in the VTK peptide increased peptide adsorption onto BLM 10-fold in comparison to nonphosphorylated VTK. While less, a significant increase in pVTK binding was also observed for the CA5 and CA10 substrates. Data are presented as means ± S.D. * denotes statistical differences between adsorption of VTK vs. pVTK on a given substrate ($p < 0.05$).

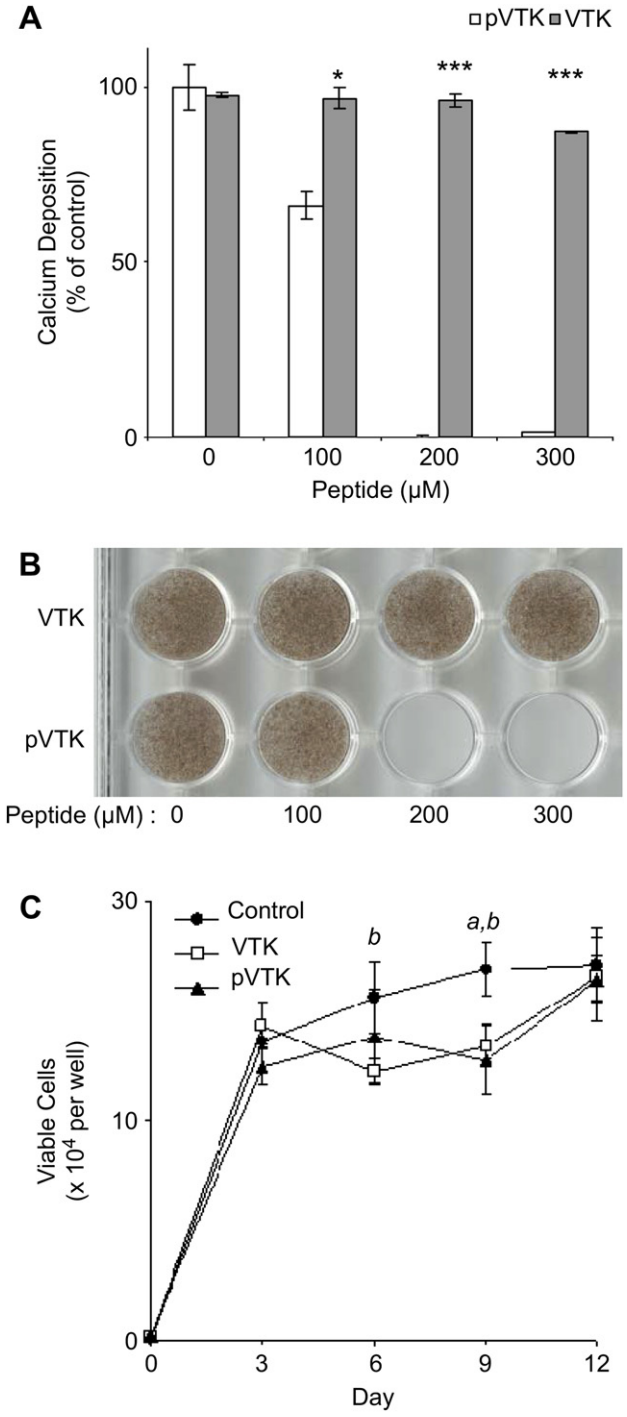

Fig. 2. Mineralizing MC3T3-E1 osteoblast cultures were incubated with VTK and pVTK at the indicated concentrations for 12 days followed by mineral quantification by (A) calcium content determination expressed as a percentage of untreated control cultures, and (B) von Kossa (silver nitrate) staining for mineral. Data are presented as means ± S.D. $*p < 0.05$; $***p < 0.001$ from Student's *t*-test for statistical differences between the two peptides at a given dose. (C) Cell proliferation in osteoblast cultures treated with, or without, 200 μM pVTK and VTK as measured by MTT assay. *a* denotes statistical significance between Control and VTK at the given time point. *b* denotes statistical significance between Control and pVTK at the given time point.

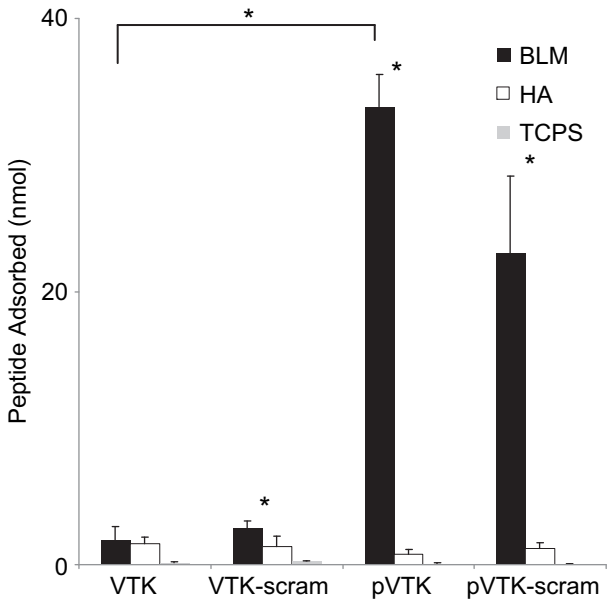

Fig. 3. Adsorption of fluorescently-labelled VTK, phosphorylated VTK (pVTK), scrambled VTK (VTK-scram) and scrambled phosphorylated VTK (pVTK-scram) on bone-like mineral (BLM), hydroxyapatite (HA) and tissue culture polystyrene (TCPS). pVTK and pVTK-scram showed significantly higher adsorption to BLM than VTK. All peptides except VTK showed significantly higher binding to BLM than HA. Substrate specificity of the peptides was confirmed by absence of binding to TCPS. Bracket denotes a statistical difference between peptides on BLM ($p < 0.05$). Data are presented as means ± S.D. * denotes statistical differences between adsorption on BLM and HA for a given peptide ($p < 0.01$).

demonstrating specificity for the apatite-based materials. Phosphorylation of VTK peptide led to a 10-fold increase in peptide adsorption to BLM relative to the nonphosphorylated peptide ($p < 0.001$). Significant increases in peptide adsorption to the carbonated disks – CA5 and CA10 ($p < 0.001$ for both CA5 and CA10) – were also observed for pVTK relative to VTK. Binding of VTK to HA was not significantly enhanced by phosphorylation. There were no significant differences in the amount of VTK adsorbed to the different apatite surfaces. However, when phosphorylated, VTK adsorption to BLM was significantly greater than to the other apatites. These data suggest that phosphorylation of amino acids on peptide sequences provides a means to control adsorption on carbonated apatite surfaces in a material/mineral-specific manner, and to increase peptide concentrations on a biomaterial surface.

3.2. Effect of VTK and pVTK on osteoblast-mediated mineralization

The MC3T3-E1 osteoblast cell line is a well-established cell culture model widely used as an *in vitro* model of osteogenesis [27,32]. MC3T3-E1 cells secrete and assemble a collagenous extracellular matrix that subsequently mineralizes over a 12-day period. To examine the effect of VTK and pVTK on osteoblast-mediated mineralization, cultures were treated with VTK and pVTK for 12 days and the mineral formed was quantified by a biochemical assay for calcium (Fig. 2A) and was visualized by von Kossa staining (Fig. 2B). pVTK dose-dependently inhibited mineralization with maximum inhibition occurring at concentrations >200 μM. Non-phosphorylated VTK had no effect on mineralization at comparable doses. Cell proliferation, as measured by the MTT assay, was reduced during days 6 and 9 of culture but was normal after 12 days of treatment with both peptides (Fig. 2C); thus, the peptides were not cytotoxic to the osteoblasts, and inhibition of mineralization attributable to toxicity was excluded.

3.3. Effects of amino acid sequence scrambling on adsorption to synthetic apatite-based substrates

To determine the role of amino acid composition versus amino acid sequence order, and therefore the role of net charge versus local charge distribution, scrambled variants of VTK and pVTK were

synthesized and their adsorption onto apatite-based substrates measured. Scrambling of the peptide sequence does not alter the net charge, but does alter the local charge distribution on the peptide, especially in the case of pVTK where the two phosphoserine residues are located close together at the N-terminus at positions 9 and 11. Scrambling VTK resulted in a significant increase in adsorption to BLM vs. hydroxyapatite, showing increased enhancement of binding specificity towards BLM (Fig. 3). Scrambling of pVTK had no significant effect on binding to either BLM or hydroxyapatite. Adsorption of scrambled pVTK was still greater than VTK or scrambled VTK, although not statistically significant. These data suggest that not only are specific residues important for binding, but that residue order may be configured to further increase binding affinity. Furthermore, the enhanced BLM binding caused by phosphorylation appears to override any further impact of a more beneficial charge distribution.

3.4. Effect of scrambled pVTK on osteoblast-mediated mineralization

pVTK-scram inhibited mineralization in osteoblast cultures with significantly less potency than pVTK (Fig. 4). Whereas pVTK exhibited a concentration-dependent inhibition and at 200 μM completely inhibited mineralization, 200 μM pVTK-scram had a significantly lesser effect on mineral inhibition. This suggests that peptide sequence order is critical for *in vitro* regulation of mineralization.

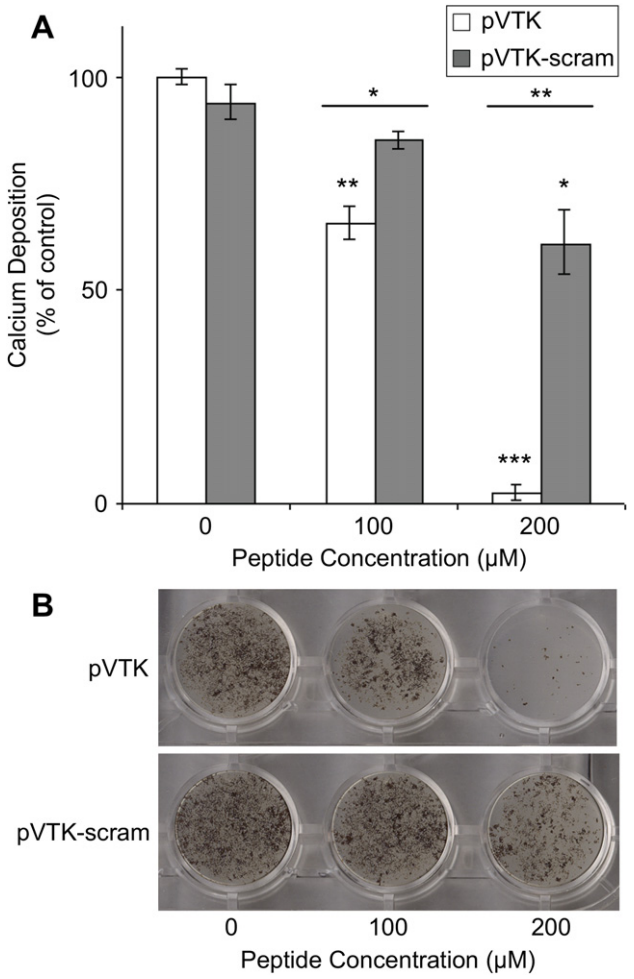

Fig. 4. Effect of scrambling pVTK on inhibition of osteoblast culture mineralization. MC3T3-E1 osteoblast cultures were treated with the indicated concentrations of pVTK and scrambled pVTK (pVTK-scram) for 12 days followed by (A) quantification of mineralization by calcium content determination expressed as a percentage of untreated control cultures, and (B) von Kossa (silver nitrate) staining for visualization of mineral. Data are presented as means ± S.D. $*p < 0.05$; $**p < 0.01$; $***p < 0.001$ from Student's *t*-test relative to the untreated control cultures or between the two peptides at a given dose (horizontal bars).

3.5. Binding of peptides to mature osteoblast culture mineral

To determine whether the increased mineralization inhibitory potency of pVTK over pVTK-scram also occurred with osteoblast mineral, mature mineralized osteoblast cultures were incubated with fluorescently-labelled peptide for 1 h, washed and visualized by immunofluorescence microscropy. Mineral was labelled with calcein blue. pVTK co-localized with the mineral, indicating strong binding whereas no fluorescence was observed for VTK, VTK-scram and pVTK-scram (Fig. 5).

3.6. Computational modeling

Computational modeling has been beneficial in the understanding of protein/peptide interactions with calcium oxalate, calcite and hydroxyapatite crystal surfaces [15,29,33,34]. The RosettaSurface protocol in particular is capable of structure predictions that are consistent with experimentally measured distances made by solid-state NMR [29]. To understand the peptide–apatite-binding observations made in this study, we used molecular modeling to calculate binding energies of VTK, pVTK, pVTK-scram and VTK-scram peptides to a high-calcium density (100) crystallographic face of hydroxyapatite. The phosphorylated peptides pVTK and pVTK-scram had significantly higher ($p < 0.001$) binding energies than the nonphosphorylated peptides (Table 2). Between pVTK and pVTK-scram however, there was no significant difference in the binding energies, suggesting that scrambling the peptide sequence did not alter binding energies. VTK and VTK-scram also had binding energies that were not significantly different. Structural prediction reveals that for pVTK and pVTK-scram the residues contributing most to the peptide–crystal surface interaction (shortest mean distance from crystal surface) were the pSer residues (Fig. 6 B and D). Despite VTK and VTK-scram having similar binding energies, the residues involved in the binding were different. For VTK, binding was mostly through the basic Lys-3 and the polar residues Gln-10 and Tyr-12, whereas for VTK-scram binding occurred via the basic Lys-5 residue (Fig. 6A and C). Fig. 6E and F show representative structures of VTK and pVTK, respectively. Lys-3 and Tyr-12 on the VTK peptide form electrostatic interactions with the crystal surface (Fig. 6E). The phosphoserine residues of pVTK coordinate with rows of calcium atoms at the crystal surface while the side-chain hydroxyl of tyrosine also interacts with the crystal surface (Fig. 6F).

4. Discussion

Phage display provides an alternative design strategy for the identification of material-specific peptides for use in functional biomaterials. Using a phage display library expressing 10^9 different peptide sequences, a 12-mer peptide – VTKHLNQISQSY (VTK) – was identified to have specificity toward apatitic mineral substrates. The affinity of a peptide for a material surface is determined by the physico-chemical properties of the individual amino acids. We therefore hypothesized that residue order and charge are design parameters that could potentially refine peptide affinity and substrate specificity. Using scrambled and phosphorylated variants of VTK, we examined the mechanisms of peptide binding to apatite-based minerals used as biomaterials, together with a functional study on the *in vitro* effects of the peptides on influencing

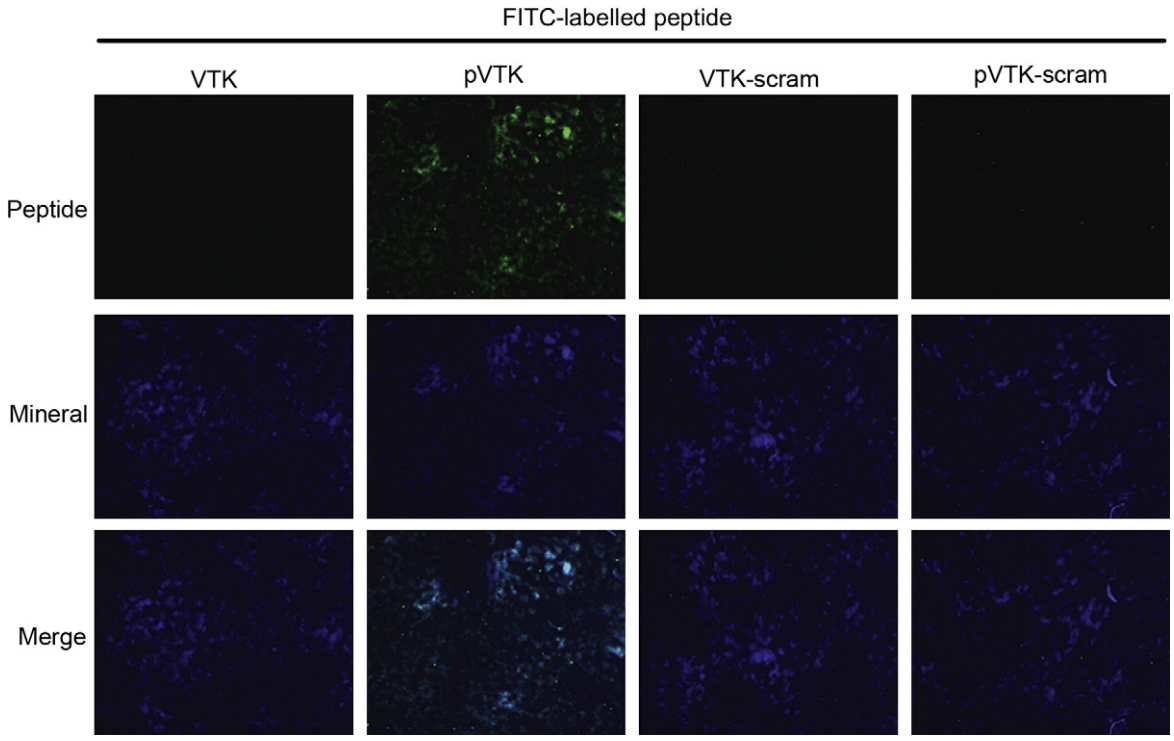

Fig. 5. Binding of peptides to osteoblast culture mineral. Maximally mineralized (12-day) MC3T3-E1 osteoblast cultures were incubated with 150 μM fluorescently tagged peptides for 1 h and examined by fluorescence microscopy for peptides (green) and calcein blue-labelled mineral (blue). pVTK co-localized with mineral indicating peptide binding to apatite.

osteoblast-mediated mineralization. The present study identifies phosphorylation manipulation as a design method to further modulate material-binding specificity. In summary, our results here show *i*) that phosphorylation increases peptide specificity for bone-like mineral and to a lesser extent carbonated apatite, *ii*) that phosphorylation is required for mineral-binding and mineralization inhibition in osteoblast cultures, *iii*) that amino acid sequence order and not simply net composition/charge play an important role in both apatite substrate binding and in osteoblast culture mineralization inhibition, and *iv*) that binding of peptides to osteoblast culture mineral depends on both peptide composition and peptide sequence.

Binding of VTK peptide to apatite was initially unexpected considering that VTK is positively charged and lacks any acidic amino acid residues; in Nature, proteins and peptides associated with mineral are typically acidic and negatively charged [12]. Phage display therefore provides a method to identify alternative, mineral-binding sequences to those already identified in naturally occurring proteins. Hydroxyapatite contains both cations and anions, so in principle there is the potential for both acidic and basic residues to bind to this mineral. Materials with high surface areas can present crystal edges as well as crystal faces. Crystal edges could provide an alternative charge distribution compared to crystal faces, further explaining the binding of the positively charged peptide to bone-like mineral. Basic residues are important for the binding of the salivary protein statherin [35] and human lysozyme to hydroxyapatite [36], and may impart specificity. Indeed, our computational modeling of VTK and VTK-scram binding to hydroxyapatite (Fig. 6) indicated the use of a variety of amino acids including the basic residue lysine and polar amino acids such as glutamine and tyrosine.

Post-translational modification of proteins, for example phosphorylation of serine, threonine or tyrosine residues, is a well-documented *in vivo* mechanism to regulate protein function [23]. We hypothesized that phosphorylation of mineral-binding peptide sequences previously identified by phage display would increase not only affinity, but specificity as well. Phosphate residues lower the isoelectric point of the molecule thereby increasing its net negative charge to favor interaction with calcium within the hydroxyapatite crystal lattice. Phosphorylation of VTK resulted in increased adsorption to bone-like mineral, and synthetic carbonato-apatite, but not to noncarbonated hydroxyapatite (Fig. 1). Furthermore, the increased affinity of pVTK for bone-like mineral was 10-fold higher than for the carbonato-apatites used here. Bone apatite differs from pure stoichiometric synthetic hydroxyapatite in that some 7% of phosphates are substituted by carbonate [37]. Futhermore, carbonate substitutions in bone and bone-like mineral are mostly Type-B (phosphate group) substitutions, whereas in the sintered hydroxyapatites and carbonato-apatites used here, the substitutions are Type-A (for hydroxyl groups) [38]. These differences in carbonate composition and location would presumably alter the surface charge distribution thereby influencing peptide affinity. Increased binding to bone-like mineral could also be related to the increased surface area or to different crystallographic face availabilities for peptide binding in BLM compared to other apatites [18]. Phosphate modifications have implications for the

Table 2
Peptide–hydroxyapatite adsorption energies calculated from Rosetta-Surface computational modeling. Binding energy is the difference between the mean energies of the 100 lowest-energy adsorbed- and solution-state candidate structures (error given is S.D.).

Peptide	Binding Energy (kcal/mol)
VTK	−4.4 ± 2.8
pVTK	−13.6 ± 5.6
VTK-scram	−4.1 ± 2.2
pVTK-scram	−14.0 ± 3.9

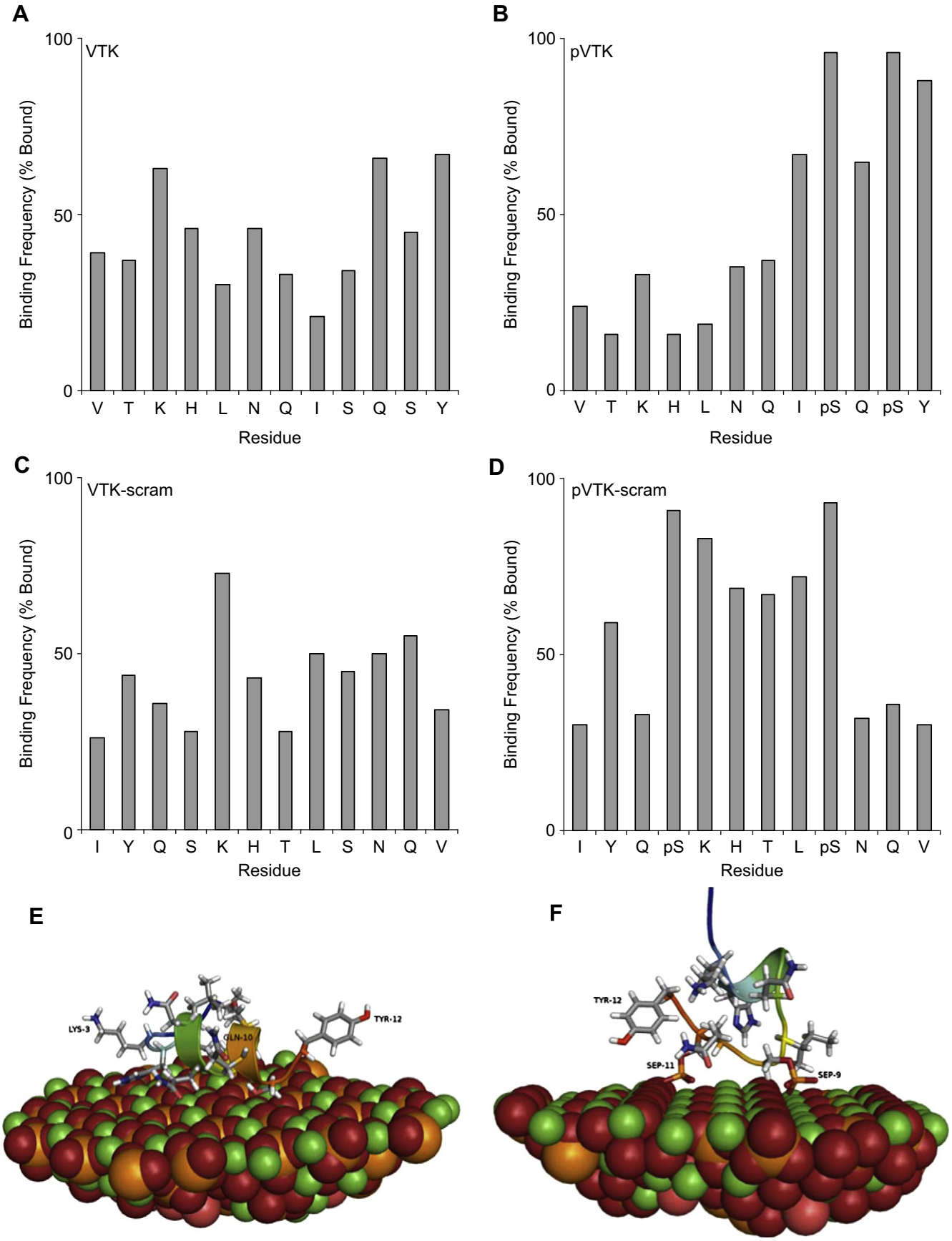

Fig. 6. Molecular modeling of peptide binding to a high-calcium density (100) crystallographic face of hydroxyapatite. (A–D) Adsorption frequency of individual residues in the 100 lowest-energy adsorbed-state structures. Bound residues are defined as residues closer than 5 Å for (A) VTK, (B) pVTK, (C) VTK-scram and (D) pVTK-scram. (E) Structural details of a representative high-scoring VTK model illustrating binding of LYS-3, GLN-10 and TYR-12. (F) Structural details of pVTK model illustrating binding of TYR-12, PSer-9 (SEP-9) and PSer-11 (SEP-11). (Ca, green; P, orange; O, red; H, white; N, blue).

tailored control of peptide binding to apatite-based materials, and phosphoserine residues in particular appear to be important in peptide interaction with carbonated apatite surfaces.

Peptide phosphorylation has been shown *in vitro* to be a mechanism by which mineralization of osteoblast cultures is controlled [34]. In the present study, we likewise observed that phosphorylation of VTK is necessary for inhibition of osteoblast culture mineralization (Fig. 2), presumably through direct binding to crystal surfaces, consistent with our cell-free, mineral-binding assays. Thus, an apatite-specific peptide may be tailored to control mineralization *in vivo* by the incorporation of phosphoserines. Inhibition of mineralization has likewise been shown for similarly sized phosphorylated osteopontin peptides in the inhibition of osteoblast culture mineralization [34], and in inhibiting hydroxyapatite [39], calcium oxalate [40] and calcite crystal growth [16].

Interestingly, we observed that scrambling of the pVTK sequence reduced its ability to inhibit mineralization (Fig. 4). These data indicate that amino acid sequence order and not just net charge is important for inhibition of mineralization. The order of amino acids determines in part the secondary structure a peptide may have, which in turn would influence its interaction with the mineral surface. Another explanation for the reduced pVTK-scram effect on mineralization could be that although pVTK and pVTK-scram have equivalent net molecular charges, the phosphoserine residues on pVTK are both situated at the C-terminus resulting in a concentration of negative charge at one end of the peptide, and thus charge distribution may be important for mineral-binding and inhibition. In order to achieve inhibition of mineralization, the location of the phosphate residues is also a factor to be considered. Although scrambling the pVTK sequence inhibited mineralization of osteoblast cultures, scrambling did not decrease binding to mature osteoblast culture mineral (Fig. 5). It is therefore possible that inhibition of mineralization and mineral-binding is controlled by different mechanisms. It is also possible that different apatite crystal faces are exposed during different stages of mineralization and peptides exhibit crystal face specificity in their binding.

The enhanced binding of pVTK (over VTK) to bone-like mineral was reflected in the observed inhibition of osteoblast culture mineralization by pVTK. However, scrambling of pVTK reduced the inhibitory potency but did not alter bone-like mineral-binding. This discrepancy could be attributable to morphologic, compositional or charge differences between biologic mineral and bone-like mineral, and further suggests that different mechanisms are important for mineral-binding and for mineralization inhibition. These observations suggest that a peptide could be designed to bind strongly to an apatitic mineral substrate but not to prevent mineralization – something that may be desirable for select biomaterial and pharmacologic purposes.

As a final point, it is important to note that the peptides did not negatively affect cell numbers after 12 days of culture and thus were not cytotoxic. Lack of toxicity supports the potential therapeutic use of peptides such as those examined here. The mineralization inhibitory potential of pVTK or similar peptides could be advantageously used for the management of ectopic calcifications and hypermineralization pathologies such as kidney stones, artherosclerosis and joint ankylosis.

5. Conclusions

Phosphorylation of serine residues on an apatite-binding peptide identified by phage display was used to refine peptide specificity for a variety of apatite-based substrates. We determined that phosphorylation enhances binding to bone-like mineral and to a lesser extent carbonated apatites. Sequence composition appears to be more important than sequence order for binding to synthetic apatite substrates, whereas regulation of osteoblast culture mineralization *in vitro* is determined by both sequence composition and sequence order.

Acknowledgements

These studies were funded by grants from the Canadian Institutes of Health Research (CIHR; MT11360 to MDM) and from the National Institutes of Health (NIH DE013380 and DE015411 to DHK). MDM is a member of the Jamson T.N. Wong Laboratories for Calcified Tissue Research of the Centre for Bone and Periodontal Research. WNA was the recipient of a studentship from the CIHR Training Grant in Skeletal Health Research. We also thank Dr. Jeffrey J. Gray and Dr. David L. Masica of JohnsHopkins University for assistance with the RosettaSurface computational simulations.

Appendix

Figures with essential color discrimination. Certain figures in this article, Figs. 2, 4, 5 and 6 are difficult to interpret in black and white. The full color images can be found in the on-line version, at doi:10.1016/j.biomaterials.2010.08.064.

References

[1] Shin H, Jo S, Mikos AG. Biomimetic materials for tissue engineering. Biomaterials 2003;24(24):4353–64.
[2] Hubbell JA. Bioactive biomaterials. Curr Opin Biotechnol 1999;10(2):123–9.
[3] Geesink RGT. Osteoconductive coatings for total joint arthroplasty. Clin Orthop Relat Res 2002;395:53–65.
[4] Alsberg E, Hill EE, Mooney DJ. Craniofacial tissue engineering. Crit Rev Oral Biol Med 2001;12(1):64–75.
[5] Kokubo T. Apatite formation on organic polymers by a biomimetic process. Eur J Solid State Inorg Chem 1995;32(7–8):819–27.
[6] Habibovic P, Barrère F, Blitterswijk CA, Groot K, Layrolle P. Biomimetic hydroxyapatite coating on metal implants. J Am Ceram Soc 2002;85(3):517–22.
[7] Segvich S, Smith HC, Luong LN, Kohn DH. Uniform deposition of protein incorporated mineral layer on three-dimensional porous polymer scaffolds. J Biomed Mater Res B Appl Biomater 2008;84(2):340–9.
[8] Luong LN, Hong SI, Patel RJ, Outslay ME, Kohn DH. Spatial control of protein within biomimetically nucleated mineral. Biomaterials 2006;27(7):1175–86.
[9] Shin H, Zygourakis K, Farach-Carson MC, Yaszemski MJ, Mikos AG. Attachment, proliferation, and migration of marrow stromal osteoblasts cultured on biomimetic hydrogels modified with an osteopontin-derived peptide. Biomaterials 2004;25(5):895–906.
[10] Gilbert M, Shaw WJ, Long JR, Nelson K, Drobny GP, Giachelli CM, et al. Chimeric peptides of statherin and osteopontin that bind hydroxyapatite and mediate cell adhesion. J Biol Chem 2000;275(21):16213–8.
[11] Fujisawa R, Mizuno M, Nodasaka Y, Yoshinori K. Attachment of osteoblastic cells to hydroxyapatite crystals by a synthetic peptide (Glu7-Pro-Arg-Gly-Asp-Thr) containing two functional sequences of bone sialoprotein. Matrix Biol 1997;16(1):21–8.
[12] Addadi L, Weiner S. Interactions between acidic proteins and crystals: stereochemical requirements in biomineralization. Proc Natl Acad Sci U S A 1985;82(12):4110–4.
[13] Gorski JP. Acidic phosphoproteins from bone matrix: a structural rationalization of their role in biomineralization. Calcif Tissue Int 1992;50(5):391–6.
[14] Sodek J, Ganss B, McKee MD. Osteopontin. Crit Rev Oral Biol Med 2000;11(3):279–303.
[15] Chien YC, Masica DL, Gray JJ, Nguyen S, Vali H, McKee MD. Modulation of calcium oxalate dihydrate growth by selective crystal-face binding of phosphorylated osteopontin and polyaspartate peptide showing occlusion by sectoral (compositional) zoning. J Biol Chem 2009;284(35):23491–501.
[16] Chien YC, Hincke MT, Vali H, McKee MD. Ultrastructural matrix–mineral relationships in avian eggshell, and effects of osteopontin on calcite growth in vitro. J Struct Biol 2008;163(1):84–99.
[17] Millán JL, Narisawa S, Lemire I, Loisel TP, Boileau G, Leonard P, et al. Enzyme replacement therapy for murine hypophosphatasia. J Bone Miner Res 2008;23(6):777–87.
[18] Segvich SJ, Smith HC, Kohn DH. The adsorption of preferential binding peptides to apatite-based materials. Biomaterials 2009;30(7):1287–98.
[19] Kriplani U, Kay BK. Selecting peptides for use in nanoscale materials using phage-displayed combinatorial peptide libraries. Curr Opin Biotechnol 2005;16(4):470–5.

[20] Adey NB, Mataragnon AH, Rider JE, Carter JM, Kay BK. Characterization of phage that bind plastic from phage-displayed random peptide libraries. Gene 1995;156(1):27–31.
[21] Marks C, Marks JD. Phage libraries – a new route to clinically useful antibodies. N Engl J Med 1996;335(10):730–3.
[22] Ladner RC, Sato AK, Gorzelany J, De Souza M. Phage display-derived peptides as therapeutic alternatives to antibodies. Drug Discov Today 2004;9(12):525–9.
[23] Qin C, Baba O, Butler WT. Post-translational modifications of sibling proteins and their roles in osteogenesis and dentinogenesis. Crit Rev Oral Biol Med 2004;15(3):126–36.
[24] Segvich S, Biswas S, Becker U, Kohn DH. Identification of peptides with targeted adhesion to bone-like mineral via phage display and computational modeling. Cells Tissues Organs 2009;189(1–4):245–51.
[25] Obenauer JC, Cantley LC, Yaffe MB. Scansite 2.0: proteome-wide prediction of cell signaling interactions using short sequence motifs. Nucleic Acids Res 2003;31(13):3635–41.
[26] Gasteiger E, Hoogland C, Gattiker A, Duvaud S, Wilkins MR, Appel RD, et al. Protein identification and analysis tools on the ExPASy server. In: Walker JM, editor. The Proteomics Protocols Handbook. Humana Press; 2005. p. 571–607.
[27] Wang D, Christensen K, Chawla K, Xiao G, Krebsbach PH, Franceschi RT. Isolation and characterization of MC3T3-E1 preosteoblast subclones with distinct in vitro and in vivo differentiation/mineralization potential. J Bone Miner Res 1999;14(6):893–903.
[28] Denizot F, Lang R. Rapid colorimetric assay for cell growth and survival: modifications to the tetrazolium dye procedure giving improved sensitivity and reliability. J Immunol Methods 1986;89(2):271–7.
[29] Masica DL, Gray JJ. Solution- and adsorbed-state structural ensembles predicted for the statherin-hydroxyapatite system. Biophys J 2009;96(8):3082–91.
[30] Goldberg HA, Warner KJ, Li MC, Hunter GK. Binding of bone sialoprotein, osteopontin and synthetic polypeptides to hydroxyapatite. Connect Tissue Res 2001;42(1):25–37.
[31] Ryuichi F, Yoshinori K. Preferential adsorption of dentin and bone acidic proteins on the (100) face of hydroxyapatite crystals. Biochim Biophys Acta Gen Subj 1991;1075(1):56–60.
[32] Sudo H, Kodama HA, Amagai Y, Yamamoto S, Kasai S. In vitro differentiation and calcification in a new clonal osteogenic cell line derived from newborn mouse calvaria. J Cell Biol 1983;96(1):191–8.
[33] Makrodimitris K, Masica DL, Kim ET, Gray JJ. Structure prediction of protein–solid surface interactions reveals a molecular recognition motif of statherin for hydroxyapatite. J Am Chem Soc 2007;129(44):13713–22.
[34] Addison WN, Masica DL, Gray JJ, McKee MD. Phosphorylation-dependent inhibition of mineralization by osteopontin ASARM peptides is regulated by PHEX cleavage. J Bone Miner Res 2010;25(4):695–705.
[35] Goobes G, Goobes R, Schueler-Furman O, Baker D, Stayton PS, Drobny GP. Folding of the C-terminal bacterial binding domain in statherin upon adsorption onto hydroxyapatite crystals. Proc Natl Acad Sci U S A 2006; 103(44):16083–8.
[36] Aizawa T, Koganesawa N, Kamakura A, Masaki K, Matsuura A, Nagadome H, et al. Adsorption of human lysozyme onto hydroxyapatite: identification of its adsorbing site using site-directed mutagenesis. FEBS Lett 1998;422(2):175–8.
[37] Awonusi A, Morris MD, Tecklenburg MM. Carbonate assignment and calibration in the raman spectrum of apatite. Calcif Tissue Int 2007;81(1): 46–52.
[38] Astala R, Stott MJ. First principles investigation of mineral component of bone: CO3 substitutions in hydroxyapatite. Chem Mater 2005;17(16):4125–33.
[39] Gericke A, Qin C, Spevak L, Fujimoto Y, Butler WT, Sorensen ES, et al. Importance of phosphorylation for osteopontin regulation of biomineralization. Calcif Tissue Int 2005;77(1):45–54.
[40] Hunter GK, Grohe B, Jeffrey S, O'Young J, Sorensen ES, Goldberg HA. Role of phosphate groups in inhibition of calcium oxalate crystal growth by osteopontin. Cells Tissues Organs; 2008.